Determination of Venus' interior structure with EnVision

Pascal Rosenblatt[1], Caroline Dumoulin[1], Jean-Charles Marty[2], and Antonio Genova[3]

[1]Laboratoire de Planétologie et Géodynamique, Nantes, France.

[2]CNES/GRGS, Toulouse, France.

[3]Sapienza University of Rome, Rome, Italy.

Corresponding author: Pascal Rosenblatt (pascal.rosenblatt@univ-nantes.fr)

Key Points:

- Daily radio tracking data from EnVision over six Venusian days will contribute significantly to determine Venus' gravity field.
- Spatial resolution of the gravity field of at least 170 km but as low as 120 km is achievable with the current mission design.
- Accurate estimate of the gravitational tides and precession rate will allow constraining the core size and state, and mantle viscosity.

Abstract

The Venusian geological features are poorly gravity-resolved and the state of the core is not well constrained, preventing to understand Venus' cooling history. The EnVision candidate mission to the ESA's Cosmic Vision Programme consists of a low-altitude orbiter to investigate geological and atmospheric processes. The gravity experiment aboard this mission aims to determine Venus' geophysical parameters to fully characterize its internal structure. By analyzing the radio-tracking data that will be acquired through daily operations over six Venusian days (four Earth's years), we will derive a highly-accurate gravity field (spatial resolution better than ~170 km), allowing to detect lateral variations of the lithosphere and crust properties beneath most of the geological features. The expected 0.3% error on the Love number k_2, 0.1° error on the tidal phase lag and 1.4% error on the moment of inertia are fundamental to constrain the core size and state as well as the mantle viscosity.

Plain Language Summary

Although, Earth and Venus are rocky planets with a similar size, they have evolved very differently. A comprehensive knowledge of Venus' geological history helps understanding what caused this different evolution. The EnVision orbiter mission candidate to the Medium class mission call of the ESA cosmic vision program aims to better characterize the atmospheric dynamics, the surface and the interior of the planet from the core to the crust. In this study we perform simulations of the EnVision gravity experiment, which is part of the radio science experiment, showing that this experiment is a fundamental asset to constrain the state and size of the core as well as the mantle viscosity. The expected results of this experiment will provide a valuable contribution to our understanding of Venus' geological history.

1 Introduction

Why Venus and Earth evolved so differently remains an open issue. The geological history of Venus is the most unknown among the terrestrial planets, preventing to fully understand the processes that led to its current state. The primary objectives of the EnVision mission, candidate to the M5 call of the ESA's Cosmic Vision Programme, are to determine whether Venus is geologically active today, the relationship with its atmosphere, and its interior structure (e.g. Ghail et al., 2019). The knowledge of the planetary interior is needed to better constrain its cooling history (e.g. Mocquet et al., 2011; Smrekar et al., 2018), and so to better constrain its geological evolution. Because of the lack of seismic data, of moon(s) and of a global magnetic field, the unique way to constrain Venus' interior from core to crust is to determine an accurate and well resolved gravity field.

The current solution of Venus gravity field was determined from the radio tracking data of the NASA Magellan spacecraft (e.g. Kaula, 1996; Barriot et al., 1998) and additionally of the Pioneer Venus Orbiter (PVO) (e.g. Konopliv and Sjogren, 1996; Konopliv et al., 1999). This recovered gravity field shows a non-uniform spatial resolution ranging from 540 to 170 km, preventing to fully detect the gravity signal induced by lithospheric loads as well as crustal density and thickness variations. To improve the determination of Venus' gravity is then fundamental to better understand the geological history of the planet (e.g. Anderson and Smrekar, 2006). In addition, our knowledge of the tidal component of the gravity field (i.e. the tidal Love number k_2) is limited by an uncertainty of 22% (Konopliv and Yoder, 1996), which is

not accurate enough to conclude about the Venus' deep interior structure, e.g. whether the core is solid (viscous) or liquid, what is its size and what is the viscosity of the mantle (Dumoulin et al., 2017). An accurate estimation of these geophysical quantities would help to constrain the cooling history of the planet. Besides, the gravity and the topography data can be used to estimate the crustal and elastic lithosphere thicknesses (e.g. James et al., 2013; Jimenez-Diaz, 2015, Anderson and Smrekar, 2006). However, the spatial resolution of the gravity field solution from Magellan tracking data is below degree and order 70 (270 km) for almost half of the planet, yielding to uncertainties in the crustal and lithosphere structure estimates (Smrekar et al., 2018).

The geophysical goals of the radio science experiment aboard EnVision are thus the determination of a uniform high-resolution gravity field to resolve anomalies associated with the geological features across the entire planet. An improved coverage of the planet will allow us to achieve an accuracy of the tidal Love number k_2 better than 3%, which is required to better constrain the Venus' mantle viscosity and composition (iron content) as well as the state of its core, by ruling out some combinations of these parameters in the current models of Venus interior (Dumoulin et al., 2017).

Here, we present numerical simulations of the EnVision gravity experiment to assess the quality of the Venus gravity solution that can be reached. Section 2 of this paper presents this experiment as currently designed, Section 3 displays the methodology to simulate this experiment, and Section 4 shows the expected improvement of the Venusian gravity field and of the knowledge of the interior structure of the planet. Section 5 summarizes the main results.

2 The EnVision gravity experiment

The main techniques to determine the gravity field of planets is based on the precise reconstruction of the motion of one or several orbiting spacecraft (e.g. Balmino et al., 1982; Konopliv and Sjogren, 1996; Zuber at al., 2007). The Precise Orbit Determination (POD) process consists in fitting the dynamical model of the spacecraft motion to the radio tracking data. The radiometric data are collected by Earth's based deep space stations (e.g. Holmes et al., 2008) that enable the telecommunications to measure the Doppler shift of the radio-link carrier frequency. The spatial resolution and accuracy of the gravity field solution depends on the precision and coverage of the tracking measurements as well as on the accuracy of the dynamical model, and on the spacecraft orbital altitude.

The EnVision spacecraft orbit is an elliptical orbit with an altitude range between 220 km and 515 km and an inclination of 88 degrees allowing for high-resolution mapping of the Venus gravity field. The EnVision gravity experiment relies on the two-way radio-link established on daily passages of at least 3.5 hours long, to guarantee the data download required by the EnVision payload. A very stable reference X-band frequency (at 7.1 GHz) is generated at the ground station and sent to the spacecraft, which then sends back to the station a coherent downlink frequency (X-band at 8.4 GHz) thanks to the radio-transponder of the spacecraft telecommunication system. An additional Ka-band downlink coherent frequency (32 GHz) is also sent back to Earth for supporting the telemetry volume requirements. This two-way X/X-Ka radio-link provide a precise Doppler tracking of the EnVision spacecraft over the six Venusian cycles of the mission science phase.

3 Methodology of simulations

We performed numerical simulations of the EnVision gravity experiment by accounting for a realistic scenario of the gravity experiment.

3.1 EnVision Doppler noise budget

The main source of noise in the X-band Doppler measurements between a Venusian spacecraft and the Earth is the electron content fluctuations of the interplanetary plasma along the propagation path of the radio wave (phase scintillation, Ho et al., 2008). The noise amplitude depends on the Sun-Probe-Earth (SPE) angle: the smaller this angle is, the closer the radio-path to the solar corona is and the larger is the noise. Models enable a characterization of this noise (Deep Space Network, note 202, 2019), but only a multi-frequency link would enable a full calibration (e.g. Iess et al., 2014). The EnVision tracking system provides a dual frequency on the downlink only, thus the plasma noise on the uplink remains. A floor value of 0.027 mm/s at 10 seconds Doppler count time is reached around inferior conjunctions (i.e. Venus is between the Sun and the Earth, Table S1), then increases toward superior conjunctions (i.e. the Sun is between the Earth and Venus), as a dominant source in the Doppler noise budget at SPE angles lower than 20 degrees (i.e. > 0.1 mm/s, see Table S1). Solar conjunctions occur with a synodic period of 584 Earth's days, therefore two or three periods during the mission timespan (i.e. 1458 Earth's days) will be characterized by high radio tracking noise, depending on the mission starting date with respect to the first superior conjunction (Figure S1).

In addition to the interplanetary plasma, other sources of propagation noise have to be taken into account, due to the charged particles of the Earth's ionosphere and to the propagation delay in the neutral atmosphere (troposphere). A calibration system using GNSS technics at the ESTRACK ground stations allows to correct the tropospheric effect with a residual error of 0.022 mm/s (Graziani et al., 2013, and see Table S1). The same technics can also provide an almost entire removal of the ionosphere effect. An additional source of noise is due to the frequency stability of the spacecraft radio-transponder. The current EnVision spacecraft design foresees a stability of 0.024 mm/s (Table S1), which is about 1.7 and 4.3 times worse than the Rosetta and Cassini transponder (Iess et al., 2014), respectively. However, it does not dominate the Doppler noise budget even at inferior conjunction periods (Table S1). Lower-level residual noise is due to the ground station Frequency and Time System (Asmar et al., 2005) and its mechanical stability (Notaro et al., 2020) (Table S1). The end-to-end Doppler noise budget, based on Table S1, is displayed in Figure S1 for the current design of the nominal science phase of the EnVision mission starting on June 15th 2035. It shows a total floor noise of 0.043 mm/s around the inferior conjunction periods and increases up to about 2.2 mm/s at the superior conjunction periods (Figure S1). For comparison the X/X Doppler tracking data of Magellan had an average noise around 0.1 mm/s at 10 seconds count time outside the superior conjunction period (see Figure 1 in Konopliv et al., 1999).

3.2 The EnVision orbital motion

An accurate dynamical model of the spacecraft orbital motion is also important to determine the gravity field of the planet (e.g. Rosenblatt et al., 2008; Marty et al., 2009; Konopliv et al., 1999, 2006; Genova et al., 2016; Goossens et al., 2017). A thorough modeling of all the forces driving the orbital motion of the EnVision spacecraft is taken into account. The primary effect is induced by Venus' gravitational force, including the tides exerted by the Sun on the planet (i.e. potential Love number k_2). The Love number k_2 has a real part and an imaginary part to take into account the tidal amplitude and the effect of the tidal phase lag, respectively (e.g. IERS conventions, McCarthy and Petit, 2004). The Magellan/PVO gravity solution, expanded up to degree and order 180, and its associated Love number k_2 are assumed as initial knowledge in our simulations. We assumed a value of 0.295 for the real part and of 0.0059 for the imaginary part (*i.e.* tidal phase lag angle of 0.58°, corresponding to the median value of the tidal dissipation factor Q values, expected from Venus interior structure models, see Figure 4 in Dumoulin et al. 2017 and Table S2). The gravitational perturbations induced on the spacecraft motion by the other planets of the solar system are also taken into account using a point mass representation and planetary ephemerides (Folkner et al., 2013).

The non-gravitational forces acting on the faces of the spacecraft include the atmospheric drag and the radiation pressure from the Sun and the planetary albedo and infra-red emission. A single value of the albedo and of the infra-red emission are here considered. We used the VTS3 model (Hedin et al., 1983) for the density of the Venusian atmosphere at the altitudes of the EnVision spacecraft. To compute these non-gravitational forces, we used a canon-ball shape model with a surface-to-mass ratio of 0.007 m^2/kg, which is representative of modern spacecraft design.

The numerical integration is performed by using these force models (hereafter *initial* model) over 365 successive 4-days long data-arcs to cover the 6 Venusian days or cycles

duration of the EnVision mission science phase. The initial state vector at the beginning of each data-arc is taken from the current design of the orbit of the EnVision spacecraft around Venus.

On the basis of this orbit computation, Doppler tracking data are simulated on a daily basis of 3.5 hours, and the Doppler noise is modeled as a white Gaussian noise with a standard deviation that accounts for the total budget and variabilities due to the SPE angle (Section 3.1).

3.3 Simulations of the Precise Orbit Determination process

A comprehensive set of numerical simulations is reported to support the science investigation of the EnVision gravity experiment. The numerical simulations were carried out independently with the software *Géodésie par Intégrations Numériques Simultanées* (GINS) developed by the French space agency CNES (Marty et al., 2009; Rosenblatt et al., 2012) and GEODYN (Pavlis et al., 2013). The simulation of the POD process consists first in building Doppler measurements on the basis of the perturbation of the *initial* force model (hereafter *perturbed* model) and the Doppler noise budget described in Section 3.1. The *perturbed* force model takes into account as faithfully as possible the inaccuracies of the force models leading to a realistic simulation of the gravity experiment.

The gravity field is perturbed by applying errors statistically modeled through Normal distributions with a standard deviation of 1-sigma uncertainty of the Magellan/PVO gravity solution (Konopliv et al., 1999) for each spherical harmonic coefficient. The real part of the Love number k_2 is set to 0.1, and the imaginary part to zero. Furthermore, each non-gravitational force accounts for errors by scaling randomly the *initial* model through a Normal distribution with a mean value of 1 (e.g. *initial* model) and a realistic standard deviation. The radiation forces are perturbed with a 0.03 standard deviation to consider possible inaccuracies in the spacecraft modeling (e.g. attitude, thermo-optical coefficients of the spacecraft panels) and in the radiation models. The standard deviation for the atmospheric drag is 0.3, which is representative of the average fluctuations of the Venusian thermosphere density observed on the day side (~5%) and night side (~50%), and is also representative of its day-to-day variability at 130-140 km (Müller-Wodarg et al., 2016).

A further source of dynamical errors is due to Wheel-off-Loading (WoL) maneuvers required to desaturate the reaction wheels used for the attitude control. These maneuvers may lead to uncompensated residual velocities caused by possible thrusters' misalignment. A maximum residual velocity $\boldsymbol{\Delta V}$ of 1 mm/s (uniformly distributed on the along-track, cross-track and radial directions) is predicted for the current EnVision spacecraft design. These effects are modeled by adjusting the thrust resulting from the impulsive $\boldsymbol{\Delta V}$ (Rosenblatt et al., 2004) at each daily maneuver, occurring before a tracking period to enable a correct adjustment of this residual $\boldsymbol{\Delta V}$ effect. This scenario is in line with the requirements of the mission operations.

The discrepancies between the *perturbed* and *initial* (Section 3.2) model-based Doppler data are then used to perform a least-squares fit of the force models by adjusting a set of parameters of these models. This fit is performed on each 4-day data-arc through a weighting of the Doppler data based on the assumed noise model (Section 3.1). A normal matrix is obtained for each arc, which contains the partial derivatives of the Doppler measurement with respect to local parameters for each arc and global parameters common to all arcs. The local parameters

include a scale factor for the drag force and for the radiation pressure force, the initial state vector and the three components of the residual thrust generated at each WoL event. The global parameters are the spherical harmonic coefficients of the gravity field to degree and order 180 and the Love number k_2 (real part) and its phase (imaginary part). The global solution is retrieved by combining the normal matrices of all the 365 simulated 4-day-arcs, which cover 6 entire Venus' cycles, to estimate both local and global parameters.

The drag scale factor is estimated for each arc with an average value of 1 +/- 0.017 (1-sigma) over the mission timespan, showing that the initial drag acceleration is precisely retrieved in spite of an a priori perturbation of 30%. The average value of the estimated solar pressure scale factor is 1 +/- 0.019 (1-sigma). This is a small improvement with respect to the 3% a priori perturbation but the adjustment of this force generally displays such a performance (e.g. Rosenblatt et al., 2008; Marty et al., 2009). The estimated residual thrust at each WoL event correspond to residual $\boldsymbol{\Delta V}$ solutions, which have accuracies better than 20%.

The estimated spherical harmonic coefficients of the gravity field up to degree and order 180, including the Love number k_2 (real and imaginary part), and their formal uncertainties (or errors) are shown in Section 4 to assess the performance of the future EnVision gravity experiment.

4 Venus' gravity field and interior structure

4.1 Static gravity and Love number k_2

The quality of the estimated gravity field is interpreted in terms of spatial resolution (i.e. degree strength) and uncertainty. The degree strength is the harmonic degree beyond which the error spectra is larger than the power spectra. Both spectra are computed with the root mean square values of all the coefficients and errors at each harmonic degree (Kaula, 1966). To map the spatial resolution, the local degree strength is computed from the spatially projected error of the gravity solution following the method presented in Konopliv et al. (1999).

The minimum degree strength of the EnVision gravity solution is 110 (spatial resolution of 170 km) that is obtained in the southern hemisphere (Figure 1a), and that corresponds to the maximal degree obtained with the Magellan/PVO solution (in the near-equatorial areas, Anderson and Smrekar, 2006). In the northern hemisphere the expected resolution of the EnVision solution reaches the degree 160 that enables a spatial resolution of ~120 km (Figure 1a) over regions covered with the lowest altitude of the spacecraft orbit. The spatial resolution map strongly depends, however, on the starting epoch of the science phase and on its initial orbital configuration (see supporting information S1 and Figure S2)

To further analyze the expected accuracy of the gravity solution, Figure 1b shows the gravity uncertainty map computed by considering the gravity field to degree and order 110. The uncertainties are < 20 mGal everywhere and <10 mGal for 88% of the planetary surface (Table S3), respectively. This is a significant improvement over the Magellan/PVO solution, which shows similar errors but at the lower degree of 70 (Konopliv and Sjogren, 1996).

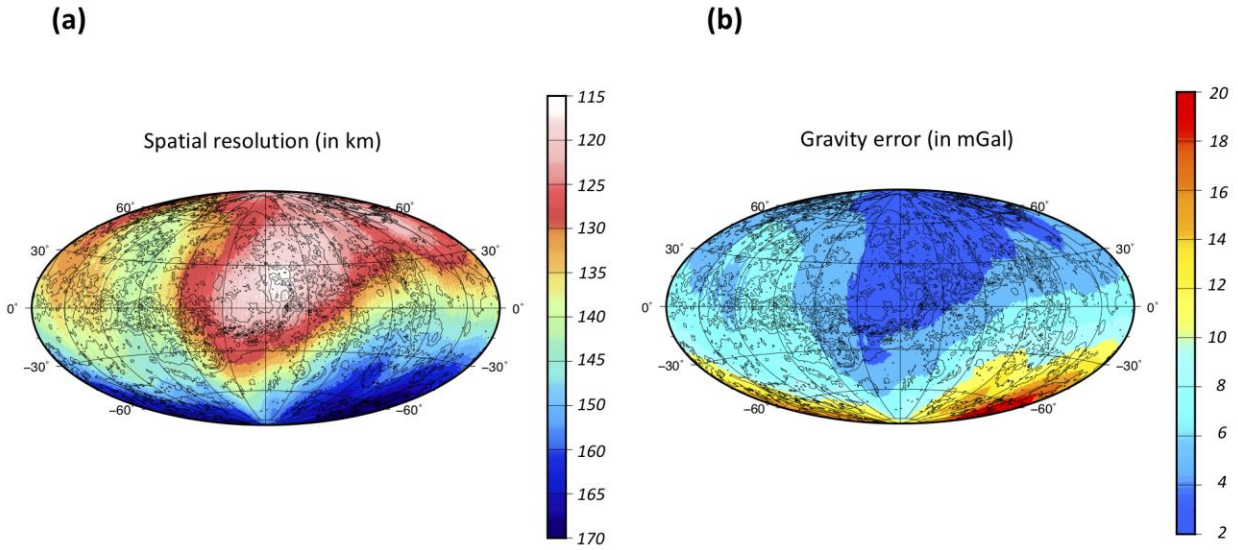

Figure 1: Expected EnVision maps (in Hammer-Aitoff projection) of (a) the spatial resolution, and (b) the cumulated gravity error (1-$\boldsymbol{\sigma}$) from the degree 2 to 110. The isocontours of the Venus topography (Rappaport et al., 1999) are shown in background.

The expected 1-$\boldsymbol{\sigma}$ error of the EnVision Love number k_2 solution is 0.001 (~0.3%) for the real part (Table S3), which is well within the required 3% error to improve our knowledge of the deep interior structure of the planet (Dumoulin et al., 2017). The 1-$\boldsymbol{\sigma}$ error of the k_2 imaginary part is 0.001, corresponding to 0.1° for the tidal phase lag error (Table S3). This error can, however, be larger because of the gravity signal due to the atmosphere (a similar issue arose in the case of Mars, Konopliv et al., 2006).

We also analyzed the effect of the mission duration (4 and 5 cycles or Venusian days instead of 6) on the performance of the gravity field resolution and accuracy as well as of the Love number k_2 and tidal phase lag solutions. The expected EnVision gravity solution is mainly affected if only 4 cycles of tracking data are available in the global inversion (Table S3). This degradation of the gravity field for this shorter mission duration is due to a less uniform surface coverage of the spacecraft ground tracks during tracking and an increased percentage of the noisier tracking data collected during solar conjunctions. A significant impact of the mission duration is also detected for the estimate of the Love number k_2 and tidal phase lag (Table S3).

4.2 Venus' interior structure

These significant improvements expected in the determination of Venus' gravity field will allow us to fully characterize the gravity anomalies associated with most of the geological features including large tesserae, volcanic rises and coronae. In particular, it will increase the coverage for crustal thickness estimates (Anderson and Smrekar, 2006), as well as the coverage of high-resolved gravity field above the coronae. Such a high resolution over all the entire

planetary surface would allow resolving gravity anomalies above more than half of the coronae. The latest gravity field solution based on the combined analysis of Magellan/POV data provides only information regarding 25% of the coronae (Hoogenboom and Houseman, 2006). This enhanced coverage of the coronae gravity signatures is required to fully understand the potential role of these structures to initiate subduction of the Venusian lithosphere (Davaille et al., 2017).

Moreover, a uniformly high-resolved gravity map will enable the analysis of the lateral variations of the elastic lithosphere thickness related to local heat flux variations (e.g. Smrekar, 1994; Anderson and Smerkar, 2006). Was the lithosphere thinner in the past, at the time of Tesserae formation and thicker at the time of more recent volcanic rises formation or could similar geological features form above lithosphere with various thicknesses? By addressing this outstanding question, we will be able to constrain the heat loss mechanism: episodic vs equilibrium mode or a different mode (e.g. Smrekar et al., 2018).

The most powerful tool to characterize the radial structure of a planet (besides seismology) is its moment of inertia, the calculation of which requires the measurement of the precession rate. The moment of inertia of Venus has been computed using estimations of the precession rate derived from Earth-based observations of radar speckles, with an uncertainty of the order of 10% (Margot, 2019). This is however not accurate enough to distinguish between the different composition models proposed in the literature for Venus that arise from different accretion scenarios (the two end-member scenarios in terms of FeO mantle content and therefore in terms of core size are the models proposed by Lewis (1972) and Ringwood (1977)). These models, combined with two different temperature profiles in the mantle (Earth-like or hotter) and assuming a core composition similar to Earth's, yield core radii from 2941 to 3425 km with corresponding moments of inertia from 0.342 to 0.327 (Dumoulin et al, 2017). In our simulations, we have introduced the estimation of the precession rate from the Envision tracking data. We found a 1-$\boldsymbol{\sigma}$ error of 70 arcsec.cy^{-1}, leading to a significant improvement of the error on the polar moment of inertia (1-$\boldsymbol{\sigma}$=0.005, that is 1.4% of the central value of the expected range) that allows a tighter constraint on the core size.

As shown in Figure 2, an accuracy of less than 2% (i.e., of the order of ± 0.006) for the Love number k_2 helps to determine bounds on the core size. Assuming a fully liquid core, a small Love number k_2 (0.25-0.27) would be the signature of a core size in the lower bound (<3000 km) and of an average viscosity of the mantle larger than 10^{20} Pa s. On the contrary, a large Love number k_2 (0.33-0.35) would be the signature of a large core (>3300 km) and of a low average viscosity of the mantle (<10^{20} Pa s). Considering a mantle composition similar to the Earth and intermediate value for mantle viscosity (10^{21} Pa s), a low value of Love number k_2 (<0.27, see Dumoulin et al., 2017) would indicate that the core is entirely solid, with a viscosity in the lower bound of Earth's inner core estimates (<10^{17} Pa s). In any case, thermal evolution modeling of mantle and core is needed in order to rule out some combinations of the state and size of the core, and of the thermal state and composition of the mantle. The determination of the tidal phase lag or Q tidal dissipation factor further constrains these parameters. The error $\boldsymbol{\sigma_Q}$ on Q is indeed lower than the range ΔQ for different averaged mantle viscosity values expected from Venus interior models (Table 1 and Figure S3). This expected error on Q will allow to further constrain the averaged viscosity within one order of magnitude (see figure 4 in Dumoulin et al., 2017) and along with the k_2 Love number, and the moment of inertia will allow us to place

even more constraints on the thermal state and composition of the interior of the planet (Figure 2).

Table 1: Expected error (1-$\boldsymbol{\sigma}$) $\boldsymbol{\sigma_Q}$ of the EnVision solution and theoretical range ΔQ of the Venus tidal dissipation factor Q as a function of the averaged mantle viscosity (see Table S2). The $\boldsymbol{\sigma_Q}$ error is derived from the error on the tidal phase angle $\boldsymbol{\delta\epsilon}$ (0.1° or 0.0017 radian, see Table S3) as follows: $\boldsymbol{\sigma_Q \approx 2Q^2\delta\epsilon}$

Averaged viscosity (Pas.s)	σ_Q *(EnVision)* *(1-*$\boldsymbol{\sigma}$*)*	Q +/- ΔQ *(Model)*
10^{22}	24.5	85 +/- 35
10^{21}	8.5	50 +/- 13.75
10^{20}	2.5	27.5 +/- 5
10^{19}	0.9	16.25 +/- 3.75

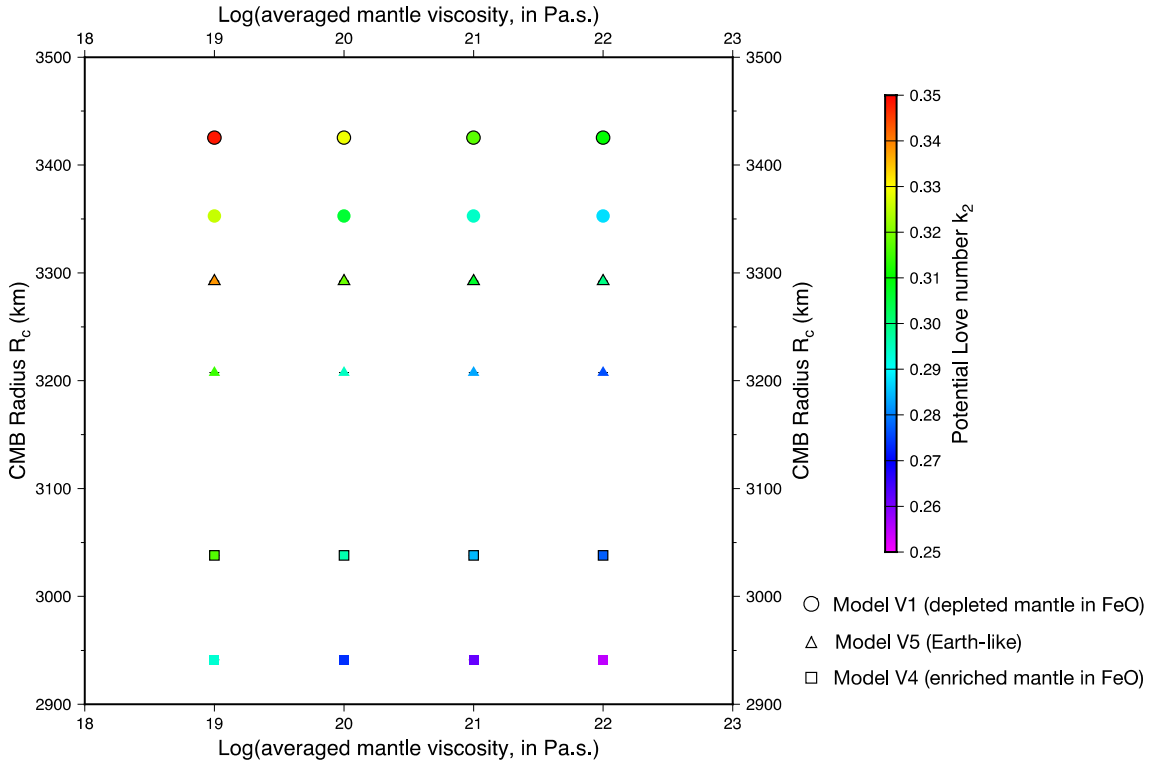

Figure 2 : k_2 Love numbers computed for a viscoelastic tidal deformation of Venus as a function of the core size and the averaged mantle viscosity. Three different composition models are tested and two different temperature profiles (an Earth-like profile, symbols with contours, and one hotter, without contours). See Dumoulin et al. (2017) for a complete description of the computation method, composition models and temperature profiles.

5 Conclusion

The EnVision Radio-Science Experiment aims at providing a global mapping of Venus' gravity field including an accurate estimation of the gravitational tides. The experiment is based on the processing of the radio-tracking data acquired by Earth's ground stations during tracking passes dedicated to telemetry and download of the mission payload data. The numerical simulations of the EnVision mission scenario demonstrates the scientific achievements that can be accomplished by the Radio Science Experiment with the configuration under study. The resulting gravity field will provide significant accuracy and resolution refinements compared to the Magellan/PVO Venus gravity field. A better Doppler tracking noise (X/X-Ka link against X/X link on Magellan), and especially the six cycles mission duration (against the three cycles dedicated to the gravity field with Magellan) enables dramatic improvements in the knowledge of the short-wavelength gravitational anomalies. A spatial resolution of 170 km is expected globally with local resolutions of 120 km over extensive regions at mid-latitudes. This improvement will provide highly resolved gravity anomalies above most of the geological

features (volcanic rises, large tesserae, coronae). The improvement of the solutions of the Love number k_2 (0.3% of error), of the tidal phase lag (0.1° of error) and of the moment of inertia (1.4% of error) will allow us to better constrain the state and size of the core, as well as the viscosity, thermal state and composition of the mantle. This improvement of the Venus interior structure will then help to better constrain the thermal evolution of the planet, providing a valuable contribution to the EnVision mission.

Acknowledgments, Samples, and Data

The Authors thank the ESA's EnVision study team for numerous and fruitful exchanges for implementing the gravity experiment in the Envision mission design as well as D. Rovelli (ESOC) for his valuable help to compute the Envision Doppler noise budget. This work was supported by CNES during the Phase A of the EnVision mission. A.G. was financially supported by the Italian Ministry of Education, University and Research (MIUR).

Data were not used, nor created for this research.

References

Anderson, F.S., & Smrekar, S.E. (2006). Global mapping of crustal and lithospheric thickness on Venus. *Journal of Geophysical Research, 111(E8),* 1-20. doi:10.1029/2004JE002395

Asmar, S.W., Amstrong, J.W., Iess, L., Tortora, P. (2005). Spacecraft Doppler tracking: Noise budget and accuracy achievable in precision radio science observations. *Radio Science, 40(RS2001),* 1-9. doi:10.1029/2004RS003101.

Balmino, G., Moynot, B., & Vales, N. (1982). Gravity model of Mars in spherical harmonics up to degree and order eighteen. *Journal of Geophysical Research, 87,* 9735-9746. doi:10.1029/JB087iB12p09735

Barriot, J.-P., Valès, N., Balmino, G., & Rosenblatt, P. (1998). A 180th degree and order model of the Venus gravity field from Magellan line of sight residual Doppler data. *Geophysical Research Letters, 25(19),* 3743-3746. doi:10.1029/98GL02600.

Davaille, A., Smrekar, S.E., Tomlinson, S. (2017). Experimental and observational evidence for plume-induced subduction on Venus. *Nature Geoscience, 10(5),* 349-355.

Deep Space Network note 202 (2019). Doppler tracking. *DSN 810-005, 202, Rev. C.* Pasadena, CA: Jet Propulsion Laboratory.

Dumoulin, C., Tobie, G., Verhoeven, O., Rosenblatt, P., & Rambaux, N. (2017). Tidal constraints on the interior of Venus. *Journal of Geophysical Research: Planets, 122(6),* 1338-1352. doi:10.1002/2016JE005249

Folkner, W.F., Boggs, D.H., & Williams, J.G. (2013). Planetary ephemeris DE430. *IOM 343-R.* Pasadena, CA: Jet Propulsion Laboratory.

McCarthy, D.D., & Petit, G. (Eds). (2004). *IERS Conventions (2003),* IERS Technical Note 32, BKG, Frankfurt/Main.

Mocquet, A., Rosenblatt, P., Dehant V., & Verhoeven O. (2011), The deep interior of Venus, Mars, and the Earth: A brief review and the need for planetary surface-based measurements. *Planetary and Space Science, 59(10),* 1048-1061. doi:10.1016/j.pss.2010.02.002

379 Genova, A., Goossens, S., Lemoine F.G., Mazarico, E., Neumann G.A., Smith, D.E., et al.
380 (2016). Seasonal and static gravity field of Mars from MGS, Mars Odyssey and MRO radio
381 science. *Icarus, 272,* 228-245. doi:10.1016/j.icarus.2016.02.050

382 Ghail, R., Wilson, C.F., Widemann, T., Titov, D., Bruzzone, L., Helbert, J., Vandaele, A.-C.,
383 Marcq, E., Dumoulin, C., Rosenblatt, P., and the EnVision team (2019). EnVision M5 Venus
384 orbiter proposal. *European Planetary Science Conference-Division Planetary Science joint*
385 *meeting*, Abstract#1611-2.

386 Goossens, S., Lemoine, F.G., Rosenblatt, P., Lebonnois, S., Mazarico, E. (2017). Analysis of
387 Magellan and Venus Express tracking data for Venus gravity field. *48th Lunar and Planetary*
388 *Science Conference*, Abstract#1984.

389 Graziani, A., Crewell, S., Elgered, G., Jarlemark, P., Löhnert, U., Martellucci, A., et al. (2013).
390 Media calibration system for deep space missions: Preliminary design and technical aspects. *6th*
391 *ESA International Workshop on Tracking, Telemetry and Command Systems for Space*
392 *Applications*, Darmstadt, Germany.

393 Ho, C.M., Morabito, D.D., & Woo, R. (2008). Solar corona effects on angle of arrival
394 fluctuations for microwave telecommunication links during superior solar conjunction. *Radio*
395 *Science, 43(2),* 1-13. doi:10.1029/2007RS003620

396 Holmes, D.P., Simpson, R., Tyler, G.L., Pätzold, M., Dehant, V., Rosenblatt, P., Häusler, B.,
397 Goltz, G., Kahan, D., Valencia, J., & Thompson, T. (2008). *The challenges and opportunities for*
398 *international cooperative radio science; Experience with the Mars Express and Venus Express*
399 *Missions.* Paper presented at AIAA/AAS Astrodynamics Specialist Conference 18,
400 Proceedingt#6395.

401 Hedin, A.E., Niemann, H.B., Kasprzak, W.T., & Seiff, A. (1983). Global empirical model of the
402 Venus thermosphere. Journal of Geophysical Research, *88(A1),* 73-84.
403 doi:10.1029/JA088iA01p00073.

404 Hoogenboom, T., & Houseman, G.A. (2006). Rayleigh Taylor instability as a mechanism for
405 corona formation on Venus. *Icarus, 180(2),* 292-307. doi:10.1016/j.icarus.2005.11.001

406 Iess, L., Di Benedetto, M., James, N., Mercolino, M., Simone, L., & Tortora P. (2014). Astra:
407 Interdisciplinary study on enhancement of the end-to-end accuracy for spacecraft tracking
408 techniques. *Acta Astronautica, 94,* 699-707. https://dx.doi.org/10.1016/j.actaastro.2013.06.011

409 Kaula, W.M. (1966). Theory of satellite geodesy. Blaisdell, Waltham, M.A.

410 Kaula, W.M. (1996). Regional gravity fields on Venus from tracking of Magellan cycles 5 and 6.
411 *Journal of Geophysical Research, 101(E2),* 4683-4690. doi:10.1029/95JE02296.

412 Konopliv, A.S., & Sjogren W.L. (1996). Venus gravity handbook. *JPL publication 96-2.*
413 Pasadena, CA: Jet Propulsion Laboratory.

414 Konopliv, A.S., & Yoder, C.F. (1996). Venusian k_2 tidal Love number from Magellan and PVO
415 tracking data. *Geophysical Research Letters, 23(14),* 1857-1860. doi:10.1029/96GL01589

416 Konopliv, A.S., Banerdt, W.B., & Sjogren, W.L. (1999). Venus gravity: 180th degree and order
417 model. *Icarus, 139(1),* 3-18. doi:10.1006/icar.1999.6086

Konopliv, A.S., Yoder, C.F., Standish, E.M., Yuan, D.-N., & Sjogren, W.L. (2006). A global solution for the Mars static and seasonal gravity, Mars orientation, Phobos and Deimos masses, and Mars ephemeris. *Icarus, 182(1),* 23-50. doi:10.1016.j.icarus.2005.12.025

Lewis, J.S. (1972). Metal/silicate fractionation in the solar system. *Earth and Planetary Science Letters, 15,* 286-290. doi:10.1016/0012-821X(72)90174-4.

Margot, J.-L. (2019). Earth-based radar observations of the spin axis orientation, spin precession rate, and moment of inertia of Venus. *European Planetary Science Conference-DPS joint meeting,* Abstract#412-3.

Marty, J.C., Balmino, G., Duron, J., Rosenblatt, P., Le Maistre, S., Rivoldini, A., et al. (2009). Martian gravity field model and its time variations from MGS and Odyssey data. *Planetary and Space Science, 57(3),* 350-363. doi:10.1016/j.pss.2009.01.004

Müller-Wodarg, I.C.F., Bruinsma, S., Marty, J.-C., & Hakan, S. (2016). In-situ observations of waves in Venus's polar lower thermosphere with Venus Express aerobraking. Nature Physics, *12(8),* 767-771. doi:10.1038/nphys3733.

Notaro, V., Iess, L., Armstrong, J.W., & Asmar, S.W. (2020). Reducing Doppler noise with multi-station tracking: The Cassini test case. *Acta Astronautica,* (173), 45-52. https://doi.org/10.1016/j.actaastro.2020.04.009

Pavlis, D. E., Wimert, J., & McCarthy, J. J. (2013). *GEODYN II System Description* (vols. 1- 5). Greenbelt, MD: SGT Inc.

Rappaport, N.J., Konopliv, A.S., Kucinskas, A.B., & Ford, P.G. (1999), An improved 360 degree and order model of Venus topography. *Icarus, 139(1),* 19-31. doi:10.1006/icar.1999.6081

Rosenblatt, P., Marty, J.C., Perosanz, F., Barriot, J.P., Van Hoolst, T., & Dehant, V. (2004). Numerical simulations of a Mars geodesy network experiment: effect of orbiter angular momentum desaturation on Mars' rotation estimation. *Planetary and Space Science, 52(11),* 965-975. doi:10.1016/j.pss.2004.07.017

Rosenblatt, P., Lainey, V., Le Maistre, S., Marty, J.C., Dehant V., Pätzold, M. et al. (2008). Accurate Mars Express orbits to improve the determination of the mass and ephemeris of the Martian moons. *Planetary and Space Science, 56(7),* 1043-1053. doi:10.1016/j.pss.2008.02.004

Rosenblatt, P., Bruinsma, S.L., Müller-Wodarg, I.C.F., Häusler, B., Svedhem, H., & Marty, J.C. (2012). First ever in situ observations of Venus' polar upper atmosphere density using the tracking data of the Venus Express Atmospheric Drag Experiment (VExADE). *Icarus, 217(2),* 831-838. doi:10.1016/j.icarus.2011.06.019

Ringwood, A.E. (1977). *Composition and origin of the Earth*. Canberra, Research School of Earth Sciences Publication No 1227, Australian National University.

Smrekar, S.E. (1994). Evidence for active hotspots on Venus from analysis of Magellan gravity data. *Icarus 112(1),* 2-26. doi:10.1006/icar.1994.1166

Smrekar, S.E., Davaille, A., & Sotin C. (2018). Venus interior structure and dynamics. *Space Science Reviews, 214(5),* 1-34. doi:10.1007/s11214-018-0518-1.

456 Zuber, M.T., Lemoine, F.G., Smith, D.E., Konopliv, A.S., Smrekar, S.E., & Asmar, S.W. (2007).
457 Mars Reconnaissance Orbiter radio science gravity investigation. *Journal of Geophysical*
458 *Research, 112*, doi:10.1029/2006JE002833.